Structure insight of GSDMD reveals the basis of GSDMD autoinhibition in cell pyroptosis

Siyun Kuang[a,1], Jun Zheng[a,1], Hui Yang[a], Suhua Li[a], Shuyan Duan[a], Yanfang Shen[a], Chaoneng Ji[a], Jianhua Gan[a], Xue-Wei Xu[b], and Jixi Li[a,2]

[a]State Key Laboratory of Genetic Engineering, School of Life Sciences, Collaborative Innovation Center of Genetics and Development, Fudan University, Shanghai 200438, China; and [b]Key Laboratory of Marine Ecosystem and Biogeochemistry, Second Institute of Oceanography, State Oceanic Administration, Hangzhou 310012, China

Edited by Hao Wu, Harvard Medical School, Boston, MA, and approved August 18, 2017 (received for review May 18, 2017)

Recent findings have revealed that the protein gasdermin D (GSDMD) plays key roles in cell pyroptosis. GSDMD binds lipids and forms pore structures to induce pyroptosis upon microbial infection and associated danger signals. However, detailed structural information for GSDMD remains unknown. Here, we report the crystal structure of the C-terminal domain of human GSDMD (GSDMD-C) at 2.64-Å resolution. The first loop on GSDMD-C inserts into the N-terminal domain (GSDMD-N), which helps stabilize the conformation of the full-length GSDMD. Substitution of this region by a short linker sequence increased levels of cell death. Mutants F283A and F283R can increase protein heterogeneity in vitro and are capable of undergoing cell pyroptosis in 293T cells. The small-angle X-ray–scattering envelope of human GSDMD is consistent with the modeled GSDMD structure and mouse GSDMA3 structure, which suggests that GSDMD adopts an autoinhibited conformation in solution. The positive potential surface of GSDMD-N covered by GSDMD-C is exposed after being released from the autoinhibition state and can form high-order oligomers via a charge–charge interaction. Furthermore, by mapping different regions of GSDMD, we determined that one short segment is sufficient to kill bacteria in vitro and can efficiently inhibit cell growth in *Escherichia coli* and *Mycobacterium Smegmatis*. These findings reveal that GSDMD-C acts as an auto-inhibition executor and GSDMD-N could form pore structures via a charge–charge interaction upon cleavage by caspases during cell pyroptosis.

gasdermin D | crystal structure | autoinhibition | antibacterial activity

Pyroptotic cell death (pyroptosis) plays key roles in host defense during pathogen infection and danger signals (self or nonself). Previous studies have shown that one gasdermin family protein, GSDMD, determines cell pyroptosis and IL-1β release (1–4). The inflammatory caspases (caspase-1 and -4/-5/-11) cleave human and mouse GSDMD after Asp275 and Asp276 respectively, generating an N-terminal cleavage product (GSDMD-N) that triggers pyroptosis and the release of inflammatory cytokines IL-1β and IL-18 (1, 2).

The N-terminal domains of the gasdermin proteins GSDMD, GSDMA3, GSDMA, and GSDME can bind membrane lipids, phosphatidylserine, and cardiolipin as well as exhibit membrane-disrupting cytotoxicity in mammalian cells and artificially transformed bacteria (5–8). Recent studies show that GSDME, originally identified as "DFNA5" (deafness, autosomal dominant 5), can be cleaved by caspase-3 and can switch TNFα- or chemotherapy drug-induced apoptosis to pyroptosis (7, 9, 10). Intriguingly, all gasdermin family members share similar N-terminal domains, and these domains exhibit comparable pore-forming activity. The N-terminal domain oligomerizes with 16-symmetric protomer in membranes to form pores (5, 6, 8, 11). The crystal structure of mouse GSDMA3 shows an autoinhibited two-domain architecture (5). Although artificially engineered GSDMA3 can cause 293T cell pyroptosis, GSDMA3 is not a physiological substrate for inflammatory caspases during pyroptosis (5). Moreover, because GSDMD is prone to form high-order oligomers in the native state, there is no detailed structural information available (5, 6).

Here we report the crystal structure of the C-terminal domain of human GSDMD (GSDMD-C) and describe the mechanism of autoinhibition in cell pyroptosis. The first loop on GSDMD-C inserts into the N-terminal domain to help stabilize the conformation of the full-length GSDMD. One short region on the surface of GSDMD-N is efficient to inhibit bacteria growth. These findings reveal that GSDMD-C acts as an autoinhibition executor during cell pyroptosis.

Results

Crystallization and Structure Determination of GSDMD-C. To elucidate the structural basis of human GSDMD in cell pyroptosis, we investigated the crystal structure of the full-length (FL) protein. However, GSDMD-FL precipitated during purification when it was concentrated and showed heterogeneity in gel filtration and SDS/PAGE. Therefore, we attempted to determine the structures of the N-terminal or C-terminal domains of human GSDMD (Fig. 1*A*). Although GSDMD-N is reported to be toxic for bacteria growth and oligomerizes into pore structures in membranes, we were able to obtain some soluble proteins; however, we failed to obtain crystals. Meanwhile, we expressed and purified GSDMD-C in *Escherichia coli* cells. It came out at a peak of 12.6 mL on a Superdex G-75 column, which corresponds to a mass of 25 kDa. This clearly showed that human GSDMD-C exists as a monomer in solution (Fig. 1*B*). In addition, we were

Significance

The protein gasdermin D (GSDMD) is the physiological substrate of inflammatory caspases and plays key roles in cell pyroptosis upon microbial infection and associated danger signals. GSDMD, as well as other gasdermin members, can bind lipid and form pore structures to induce pyroptosis. However, detailed structural information for GSDMD remains unknown. We have determined the crystal structure of the C-terminal domain of human GSDMD. The structure reveals that the first loop inserts into the N-terminal domain to help stabilize the full-length GSDMD conformation. Furthermore, we identify that one short segment is sufficient to kill bacteria and can act as a potential antimicrobial peptide. Thus, these findings offer a perspective for understanding the mechanism of GSDMD in innate immune defense.

Author contributions: J.L. designed research; S.K., J.Z., H.Y., S.L., S.D., Y.S., C.J., and X.-W.X. performed research; S.K., J.Z., S.L., C.J., J.G., X.-W.X., and J.L. analyzed data; and J.L. wrote the paper.

The authors declare no conflict of interest.

This article is a PNAS Direct Submission.

Data deposition: The coordinate and structural factors have been deposited in the Protein Data Bank (PDB ID code 5WQT).

[1]S.K. and J.Z. contributed equally to the work.

[2]To whom correspondence should be addressed. Email: lijixi@fudan.edu.cn.

This article contains supporting information online at www.pnas.org/lookup/suppl/doi:10.1073/pnas.1708194114/-/DCSupplemental.

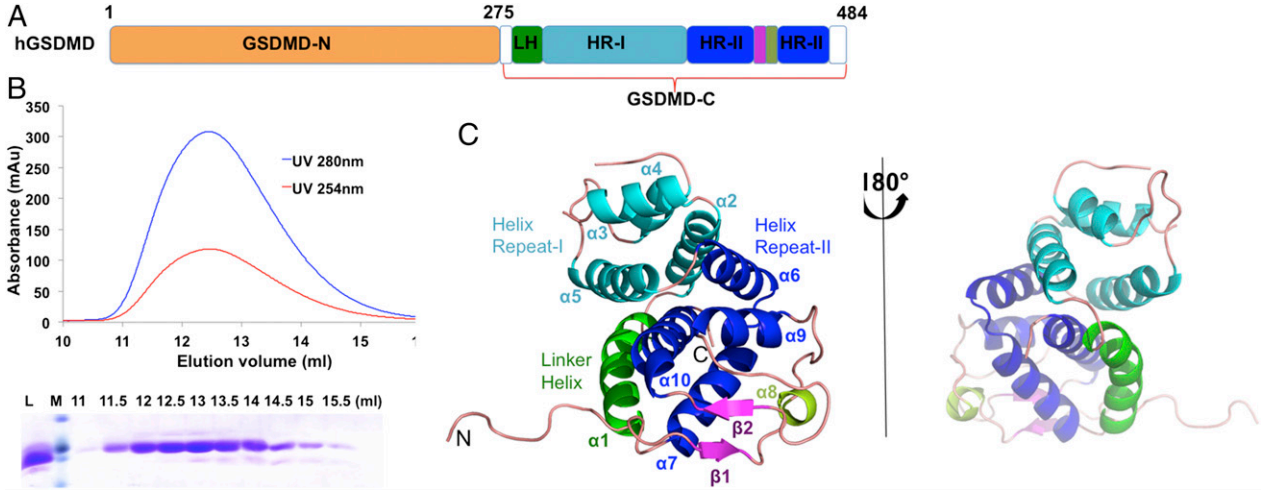

Fig. 1. Crystal structure of human GSDMD-C. (*A*) Schematics of human GSDMD domains. GSDMD is composed of two domains, the N-terminal domain, GSDMD-N, and the C-terminal domain, GSDMD-C. GSDMD-C includes four subdomains: the linker helix (LH, green), the helix repeat-I bundle (HR-I, cyan), the helix repeat repeat-II bundle (HR-II, blue), and the intermediated β-strand insertion (purple). (*B*) Gel filtration profile (*Top*) and SDS/PAGE analysis (*Bottom*) of GSDMD-C. GSDMD-C was eluted at a peak of 12.6 mL on a Superdex G-75 10/300 column. L, loading sample; M, protein marker. (*C*) A ribbon representation of the GSDMD-C structure, colored by domain structure. Secondary structures are labeled in accordance with *A*.

able to acquire crystals for GSDMD-C (residues 276–484) and solved the structure by molecular replacement method at 2.64-Å resolution using the mouse GSDMA3 structure as the search model. The final structure contains two GSDMD-C molecules per asymmetric unit, chain A (residues 277–482) and chain B (residues 276–482) (Table S1).

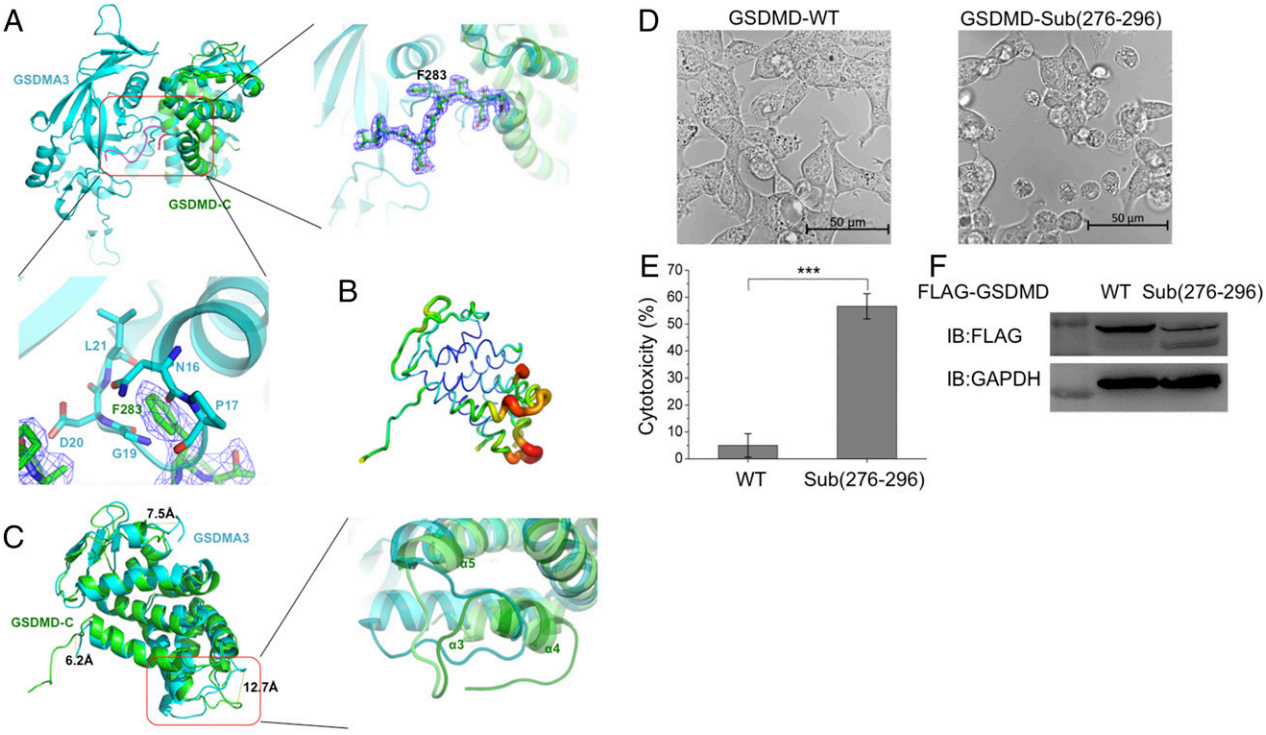

Fig. 2. Structural comparison between human GSDMD-C and mouse GSDMA3 reveals that the linker region (276–296) is important for cell pyroptosis. (*A*, *Upper Left*) GSDMD-C (green) was superimposed on the C-terminal domain of GSDMA3 (cyan). Both structures showed similar overall folds, with a major difference existing in the linker region between the N-terminal and C-terminal domains. (*Upper*, *Right*) Enlarged view of the boxed area at the left showing residue F283 inserted into the pocket formed by α1, β3, and α5 of GSDMA3. (*Lower*) This insertion might result in severe clashes with adjacent residues located on the loop region (residues 16–21) of GSDMA3. The $2F_o - F_c$ electron density map was contoured to 1.5σ. (*B*) The B-factor distribution of human GSDMD-C. The wider and darker red tubing indicates higher B-factor. (*C*, *Left*) The structure superimposition revealed three major differences between human GSDMD-C and mouse GSDMA3. (*Right*) One inserted helix α4 is absent on the mouse GSDMA3 structure, in which it forms a flexible loop. (*D*) Live images of GSDMD and its loop mutant. 293T cells were transfected with FLAG-tagged WT GSDMD or GSDMD-Sub(276–296) (in which the 276–296 region was replaced by a short linker sequence GSGGGS). (*E*) The lactate dehydrogenase (LDH) assay shows that GSDMD-Sub(276–296) has pyroptosis-induced activity. Asterisks indicate significance: ***$P < 0.001$. (*F*) Expression levels of GSDMD and GSDMD-Sub(276–296) in 293T cells.

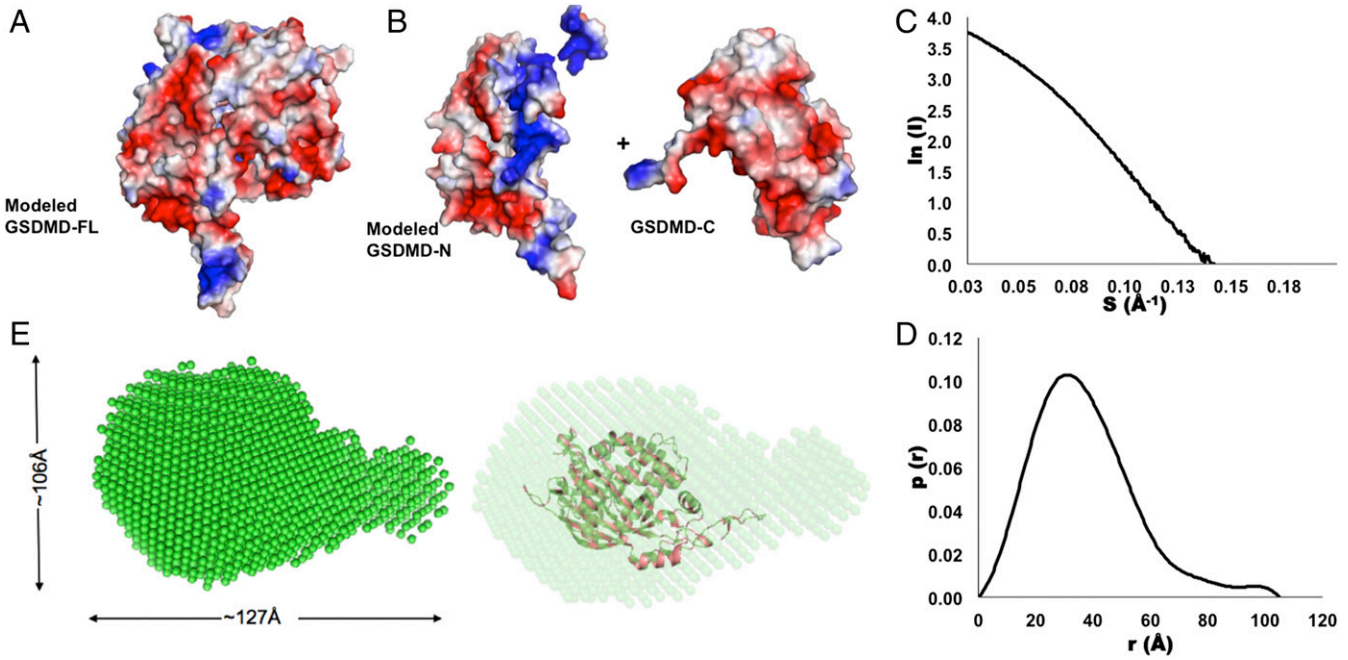

Fig. 3. The potential surface distribution and SAXS analysis of human full-length GSDMD. (*A* and *B*) The electronic potential surfaces of human GSDMD-C (*A*) and the modeled GSDMD-FL and GSDMD-N structures (*B*). Red indicates negative potential, and blue indicates positive potential. (*C* and *D*) The experimental scattering curve (*C*) and the distance distribution function curve (*D*). (*E*, *Left*) The SAXS envelope using the ab initio molecular modeling has a gourd shape. (*Right*) The modeled structure of GSDMD-FL was fitted into the SAXS envelope.

The Structure of Human GSDMD-C. The structure of GSDMD-C forms a compact globular fold comprising 10 α-helices and two β-strands. GSDMD-C can be divided into four subdomains: the linker helix; the helix repeat-I (α2–α5); the middle domain containing an inserted antiparallel β-strand and a short α helix (α8); and the helix repeat-II (α6–α7 and α9–α10) (Fig. 1*C*). One flexible loop (residues 276–287), located between the N-terminal domain and the linker helix, stretches out to the N-terminal pocket (Fig. 2*A*). The two helix-repeats (I and II) are composed of similar four-helix bundles, and the linker helix contacts the two bundles. As no visible electron density for the flexible loop between α3 and α4 (residues 335–342) was detected, this region is disordered.

Structural Comparison of GSDMD-C with GSDMA3. Mouse GSDMA3 protein [Protein Data Bank (PDB) ID code 5B5R] (6) shares a homologous sequence with human GSDMD, so we compared their tertiary structures to better understand the architecture of human GSDMD (Fig. 2*A* and Fig. S1). Superimposing GSDMD with GSDMA3 reveals similar features of overall folds, which have a high similarity with an rmsd value of 2.8 Å among 183 Cα atoms with the DALI server (ekhidna.biocenter.helsinki.fi/dali_server/start). The structural differences exist in three regions: in the first loop before α1, the loop between α4 and α5, and the loop between α8 and β2, all of which are 6.2–12.7 Å apart (Fig. 2 *B* and *C*). The GSDMD-C structure has a longer flexible loop (276–296) that inserts into the N-terminal pocket formed by α1, β3, and α5 of GSDMA3 (Fig. 2*A*). This loop is not observed in the GSDMA3 structure, as it is omitted on the electron density map. Surprisingly, residue F283 on human GSDMD-C has severe clashes with adjacent residues located on the loop region (residues 16–21) on GSDMA3. The double mutations L192D/E15K in GSDMD-N attenuate pyroptosis-inducing activity in the 293T cell line (6), which may result from the changes in the surrounding area potentially caused by the mutation. The region between α3 and α5 is largely shifted from the same region in GSDMA3, and the inserted helix α4 is absent on the mouse GSDMA3 structure, in which it forms a flexible loop (Fig. 2*C*).

The full-length GSDMD does not induce cell pyroptosis, whereas GSDMD-N has pyroptosis-inducing activity (1); thus we hypothesize that the loop (276–296) could help stabilize the overall structure of GSDMD. Indeed, when the loop was replaced by a short linker sequence, GSGGGS, which does not change the protein quaternary structure (12), it dramatically induced cell death in 293T cells (Fig. 2 *D*–*F*). This showed that the first loop could help stabilize the autoinhibition between the N- and C-terminal domains of GSDMD.

High-Order Oligomer Forming via Charge–Charge Interaction. The charge–charge interaction accounts critically for protein stacking in many high-order oligomers and filament formation (13–17). GSDMD-N forms pore structures after cleavage by inflammatory caspases at residue D275 when binding with lipids (5, 6). Therefore, we wanted to determine the order in which pore structure formation and lipid binding occur. We checked the structural surface and found that the GSDMD-C is full of negative potential surface (Fig. 3 *A* and *B*). In contrast, the modeled GSDMD-N domain has two different charged surfaces, and the positive charge surface is exposed when cleaved by caspases (Fig. 3 *A* and *B*). The positive potential pole or pocket surface on GSDMD-C can bind lipids and therefore induce the formation of high-order oligomers via a charge–charge interaction.

In addition, we investigated GSDMD-FL using the small-angle X-ray–scattering (SAXS) method. The SAXS pattern of the GSDMD-FL in solution was recorded to generate a final composite scattering curve. The radius of gyration (Rg) is 29.39 Å, and the maximum dimension (D_{max}) from the distance distribution function p(r) is 104.89 Å (Fig. 3 *C* and *D*). The SAXS envelope of human GSDMD-FL reconstructed from the scattering pattern appears to be gourd-shaped with a large section and a small one (Fig. 3*E*). When the modeled human GSDMD structure was fitted into the SAXS envelope, the two structures showed similar but narrow dimensions, which could result from high flexibility of GSDMD-FL; similar phenomena have been observed in many other proteins (Fig. 3*D*) (18).

It is difficult to obtain the GSDMD-FL crystal structure, so we attempted to determine the homogeneity of GSDMD with native

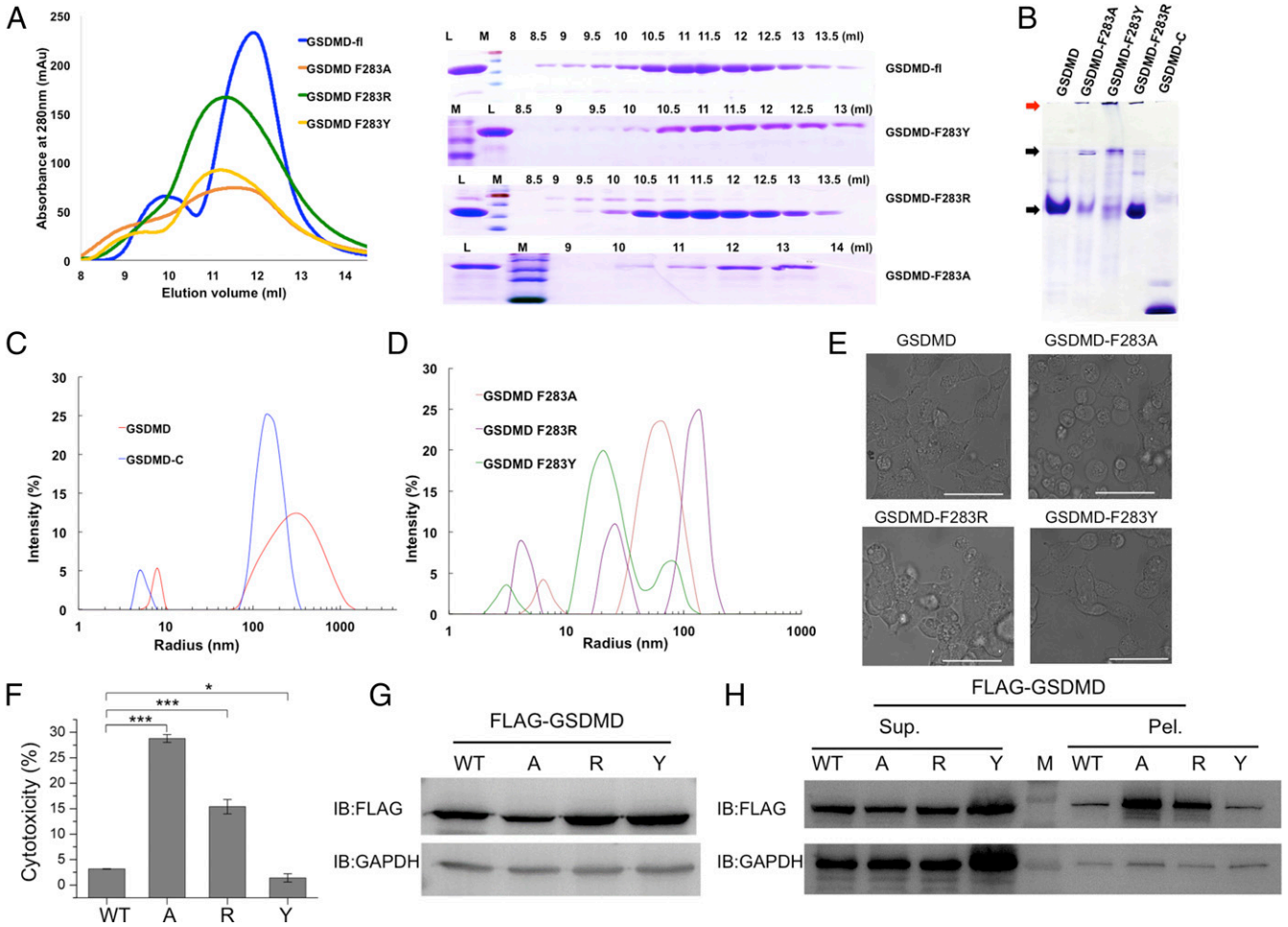

Fig. 4. The properties of WT GSDMD and its mutants. (*A*) The gel-filtration profiles of WT and mutants (*Left*) and the corresponding SDS/PAGE result (*Right*). L, loading sample; M, protein marker. (*B*) The native PAGE of human GSDMD and its mutants. The low molecular weight proteins and the aggregated proteins are identified by black and red arrows, respectively. (*C* and *D*) DLS analysis of human GSDMD-C and full-length GSDMD (*C*) and the mutants of GSDMD (*D*). (*E*) Live images of GSDMD and its F283A, F283R, and F283Y mutants. 293T cells were transfected with FLAG-tagged WT GSDMD or its mutants. (Scale bars, 50 μm.) (*F*) The LDH assay shows that the F283A or F283R mutation induced cell pyroptosis. A, F283A mutation; R, F283R mutation; Y, F283Y mutation. Asterisks indicate significance: $*P < 0.05$; $***P < 0.001$. (*G*) The whole-cell protein expression levels of GSDMD and its mutants in 293T cells. (*H*) Expression levels of GSDMD and its mutants with supernatant/pellet fractionation, corresponding with *G*. Mutant A has a higher protein expression level in precipitation even though the whole-cell expression is lower than in WT or other GSDMD mutants.

PAGE and dynamic light-scattering (DLS) methods. Because the residue Phe283 might interact with amino acids on the loop of the GSDMD N-terminal region, we mutated it to residues Ala, Arg, or Tyr to check whether it clashed with the packing pattern between the N-terminal and C-terminal domains (Fig. 4*A*). All proteins were expressed well, and most WT GSDMD protein was in a monomeric state, with small portions as a dimer or high-order oligomer (Fig. 4*B*). However, the mutants F283A, F283Y, and F283R shifted mostly to the high-order oligomers and could not enter the stacking gel when analyzed by SDS/PAGE (Fig. 4*B*). In the DLS experiment, the size distribution of human GSDMD shifted from a large radius to a small one (Fig. 4 *C* and *D*). The mean hydrodynamic diameter and percent of polydispersity (% Pd) of WT GSDMD were 7.9 nm and 9.2, respectively. Compared with the WT GSDMD, F283A had a lower % Pd value, whereas F283Y and F283R had higher values. In addition, F283A had a larger radius than the other two mutants, which meant that the F283A particles were less monodispersed (Table S2).

To further identify the potential function of residue F283, we transfected these mutated constructs into 293T cells. Interestingly, mutants F283A and F283R clearly induced cell death, whereas F283Y did not affect cell viability (Fig. 4 *E* and *F*). We then checked their expression levels with anti-FLAG antibody. Not surprisingly, mutants F283A and F283R had low levels in whole cells compared with WT and F283Y (Fig. 4*G*). Interestingly, after we did the fractionation assay for supernatant and pellets, most portions of F283A and F283R existed in cell pellets, whereas all mutants had similar expression levels in supernatants. Together, these results suggested that the linker on the first loop region could undergo large conformational changes, leading to different oligomeric statuses, and, in contrast to the stable monomeric WT protein, the F283A and F283R mutants had intrinsic properties to form high-order oligomers.

The Minimal Region for Antibacterial Toxicity and Potential for Forming Amyloid Fibrils. Previous reports showed that the GSDMD-N region has antibacterial activity but does not kill human cells (5, 6); however, we do not know the exact region controlling this activity. To identify the minimal region and investigate it as a potential antimicrobial peptide, we transformed different fragments fused with a His-SUMO tag on the pSMT3 vector into *E. coli* cells. After 20 h of incubation at 37 °C, we found that the minimal region was mapped to a short segment (residues 80-FHFYDAMDGQI-90) and that it was

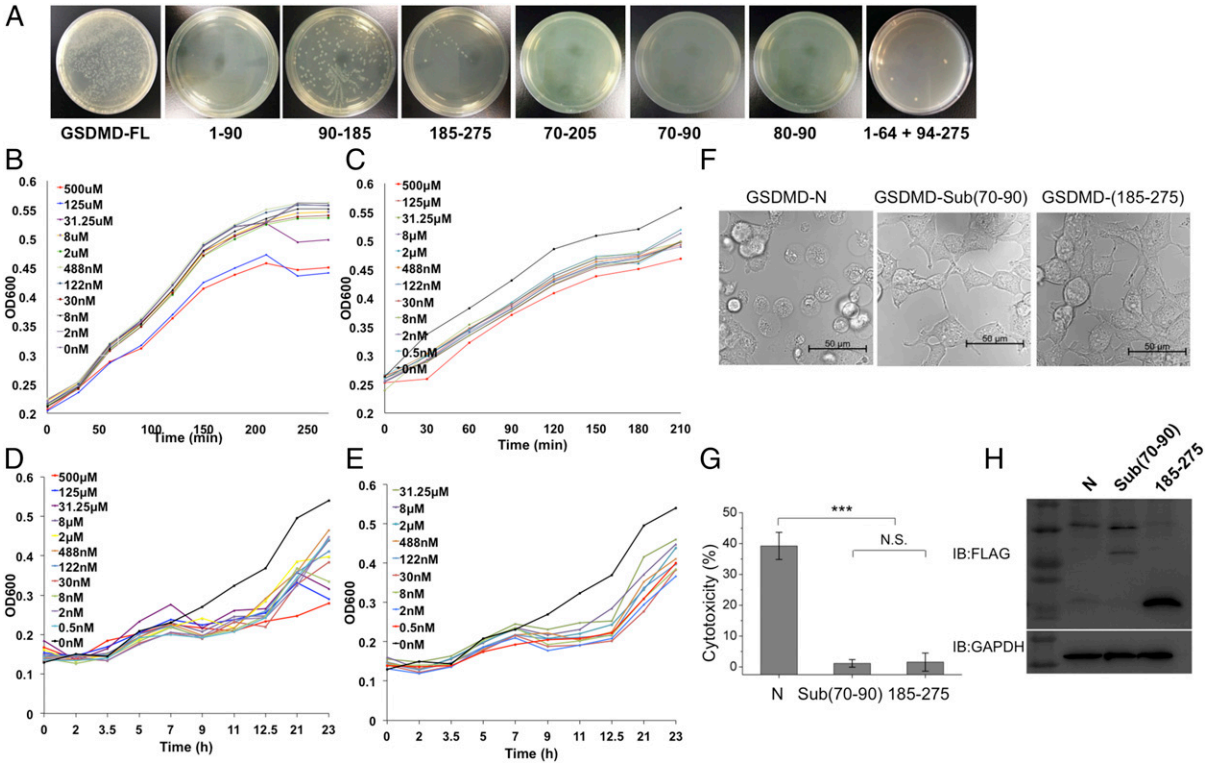

Fig. 5. Identification of the antibacterial peptides of GSDMD. (*A*) The *E. coli* cells transformed with WT and truncated GSDMD were incubated at 37 °C for 20 h. The data showed that the short regions (residues 80–90 and residues 70–90) are sufficient to inhibit bacterial growth. (*B* and *C*) The effects of two synthesized peptides, FHFYDAMDGQI (*B*) and AEPDVQRGRSFHFYDAMDGQI (*C*), on the growth of *E. coli* host strains. The peptide sequences are the same as the two regions in GSDMD. (*D* and *E*) The effects of two synthesized peptides, FHFYDAMDGQI (*D*) and AEPDVQRGRSFHFYDAMDGQI (*E*) on the growth of *M. smegmatis* host strains. Serial dilutions of the peptides with final concentrations of 500 μM, 125 μM, 31.25 μM, 8 μM, 2 μM, 488 nM, 122 nM, 30 nM, 8 nM, 2 nM, and 0 nM were added to the LB media (*B* and *C*) or to Middlebrook 7H9 broth with OADC enrichment (*D* and *E*) cultures. The growth curves were determined by measuring the OD at 600 nm. (*F*) Live images of GSDMD-N and its mutants. 293T cells were transfected with FLAG-tagged GSDMD-N, Sub(70–90) (in which residues 70–90 were replaced with a linker sequence GSGGGS), or the truncated version 185–275. (*G*) The LDH assay shows that substitution of residues 70–90 abolished pyroptosis-induced activity. ***$P < 0.001$; N.S., not significant. (*H*) Expression levels of GSDMD-N and its mutants in 293T cells.

sufficient to kill bacteria (Fig. 5*A*). In addition, two synthesized peptides based on residues 80–90 and residues 70–90 of GSDMD inhibited the growth of *E. coli* and *Mycobacterium smegmatis* in vitro (Fig. 5 *B*–*E*). Peptide 1 (residues 80–90) inhibits *M. smegmatis* growth at a low concentration of 2 nM (Fig. 5*D*) but requires a minimal concentration of 31.25 μM to inhibit *E. coli* cell growth (Fig. 5*B*). Peptide 2 (residues 70–90) has a better inhibition capability and can inhibit *E. coli* and *M. smegmatis* growth at a concentration of 2 nM (Fig. 5 *C* and *E*). These data suggest that peptide 2 from human GSDMD has the potential to be an excellent antimicrobial peptide.

To identify whether this region (residues 70–90) is important for cell viability, we replaced it with a short linker sequence,

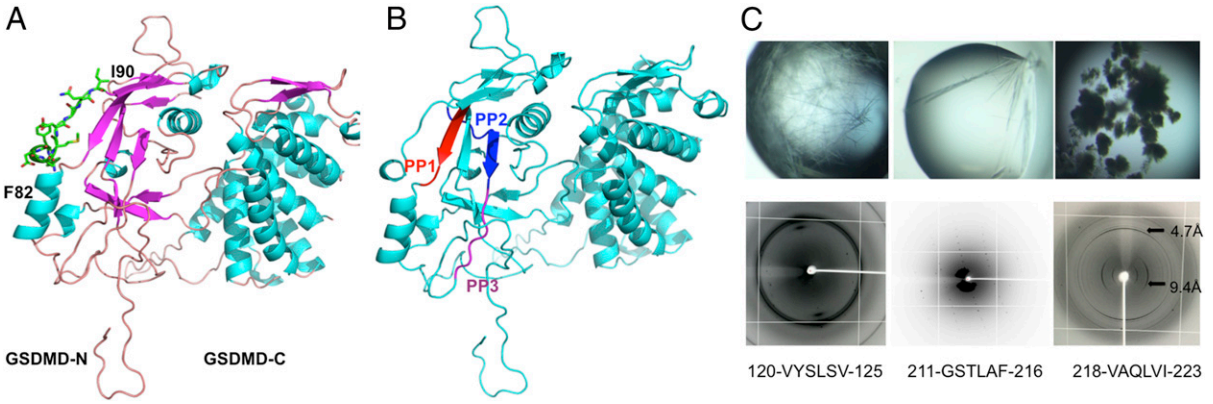

Fig. 6. The amyloid-forming segments of human GSDMD. (*A*) The loop region (residues 82–90) is shown by sticks on the modeled GSDMD structure. (*B*) The three amyloid-forming segments are labeled as PP1 (120-VYSLSV-125, red), PP2 (211-GSTLAF-216, blue), and PP3 (218-VAQLVI-223, purple), respectively. (*C*) The three short segments are prone to form amyloid fibrils. (*Upper*) Needle-like crystals. (*Lower*) X-ray diffraction patterns. The perpendicular rings at 4.7 Å and 9.4 Å represent a typical amyloid diffraction pattern. (Magnification: *Upper*, 80×; *Lower*, 2×.)

GSGGGS, and transfected it into 293T cells. GSDMD-N triggered significant cell death, as previously reported (1, 2). Correspondingly, the substitution of this region (residues 70–90) and one truncated construct of GSDMD (residues 185–275) did not affect cell viability (Fig. 5 *F–H*). When checked with anti-FLAG blots, both GSDMD-N and the substitution had lower expression levels than the truncated one that did not affect cell death.

To further investigate the possible function of peptide 2 in GSDMD, we obtained the modeled GSDMD-FL structure using the SWISS-MODEL server. This region is located on the surface, forming a flexible loop (Fig. 6*A*); however, the corresponding short region (residues 70–81) is disordered in the mouse GSDMA3 structure (5). Additionally, because GSDMD-N has lipid-binding preferences, it kills from within the cell but does not harm neighboring mammalian cells when it is released during pyroptosis (6). Thus, this region could mediate the interaction between GSDMD and lipids on the cell-membrane surface.

One intriguing attribute of molecules involved in cell death (necroptosis and pyroptosis) is that most proteins have the potential to form high-order oligomers or amyloid-like fibrils (13, 19, 20). Thus, we propose that human GSDMD could have the capability to form high-order oligomers via short segments. After screening the full-length sequence of human GSDMD with the prediction server ZipperDB (19), we identified three short segments with energy below −25 kcal/mol that were predicted to form fibrils (Fig. 6*B*). Indeed, two segments (120-VYSLSV-125 and 211-GSTLAF-216) grew into needle-like crystals with a typical X-ray diffraction model (Fig. 6*C*). The other segment formed fibrils and was confirmed to form two perpendicular diffraction rings, corresponding to the reported β-amyloid pattern (21). The high-order oligomer or fibril can act as a platform to amplify signals in innate immunity (16). However, the functions of these segments need to be further investigated.

Discussion

Current studies show that cell pyroptosis can be referred to as "gasdermin-mediated programmed necrotic cell death" (1, 2, 5–8, 11, 22). Because of their physiological functions, gasdermins have emerged as a new class of molecules that could induce cell death for clearing bacterial infection. GSDMD is the physiological substrate of inflammatory caspases. Although the structures of mouse GSDMA3 and the C-terminal domain of GSDMB have been solved (5, 23), our crystal structure of GSDMD-C reveals that the linker loop between the N-terminal or C-terminal domains plays essential roles in stabilizing the autoinhibited GSDMD. The short linker GSGGGS substitution did not change the quaternary structure (12); however, it induced cell death, which might be due to the release of autoinhibition between the N- and C-terminal domains of GSDMD. Our structure also showed that F283 could help stabilize the autoinhibition, whereas the single mutation F283A or F283R abolished the interaction between the N- and C-terminal domains and therefore increased levels of cell death. The F283Y mutation did not increase cell death level, probably due to the hydrogen bonds formed by tyrosine with other adjacent residues.

Our biochemical studies identified the minimal region controlling antibacterial activity and the segments that tend to form amyloid-like fibrils. When this region was replaced with a GSGGGS linker, the cytotoxicity of GSDMD-N was abolished even though the protein expression level did not change significantly. A previous report mentioned that amyloid-β peptide protects against microbial infection in innate immunity besides its damaging roles in the brain (24). Whether the short region of GSDMD could work in a similar way remains unknown. Many other studies have shown that amyloid-like proteins, including amyloid-β, HET-s, α-synuclein, and IAPP, can form multiple types of filamentous structures, such as amyloid pores and fibrils (25–29). GSDMD-N forms pore structures (5, 6, 8, 11); however, whether the pores can be changed into fibrils needs to be further investigated. All these findings may increase our understanding of how the gasdermin family proteins function in cell pyroptosis and innate immune defense.

Materials and Methods

For detailed experimental procedures, please see *SI Materials and Methods*.

ACKNOWLEDGMENTS. We thank the staffs of the Shanghai Synchrotron Radiation Facility beamline BL17U1 and the National Center for Protein Science Shanghai beamlines BL19U1 and BL19U2 for help with X-ray and SAXS data collection. This work was supported by National Key Research and Development Program of China Grants 2016YFA0500600 and 2015CB943300, National Natural Science Foundation of China Grants 31470724 and 31670878, and Program for Professor of Special Appointment (Eastern Scholar) Grant TP2014010 to J.L.

1. Shi J, et al. (2015) Cleavage of GSDMD by inflammatory caspases determines pyroptotic cell death. *Nature* 526:660–665.
2. Kayagaki N, et al. (2015) Caspase-11 cleaves gasdermin D for non-canonical inflammasome signalling. *Nature* 526:666–671.
3. Shi J, Gao W, Shao F (2017) Pyroptosis: Gasdermin-mediated programmed necrotic cell death. *Trends Biochem Sci* 42:245–254.
4. He WT, et al. (2015) Gasdermin D is an executor of pyroptosis and required for interleukin-1beta secretion. *Cell Res* 25:1285–1298.
5. Ding J, et al. (2016) Pore-forming activity and structural autoinhibition of the gasdermin family. *Nature* 535:111–116.
6. Liu X, et al. (2016) Inflammasome-activated gasdermin D causes pyroptosis by forming membrane pores. *Nature* 535:153–158.
7. Wang Y, et al. (2017) Chemotherapy drugs induce pyroptosis through caspase-3 cleavage of a Gasdermin. *Nature* 547:99–103.
8. Aglietti RA, et al. (2016) GsdmD p30 elicited by caspase-11 during pyroptosis forms pores in membranes. *Proc Natl Acad Sci USA* 113:7858–7863.
9. Van Laer L, et al. (1998) Nonsyndromic hearing impairment is associated with a mutation in DFNA5. *Nat Genet* 20:194–197.
10. Rogers C, et al. (2017) Cleavage of DFNA5 by caspase-3 during apoptosis mediates progression to secondary necrotic/pyroptotic cell death. *Nat Commun* 8:14128.
11. Chen X, et al. (2016) Pyroptosis is driven by non-selective gasdermin-D pore and its morphology is different from MLKL channel-mediated necroptosis. *Cell Res* 26:1007–1020.
12. Liu Z, Wang Z, Chen YH (2005) Predefined spacers between epitopes on a recombinant epitope-peptide impacted epitope-specific antibody response. *Immunol Lett* 97:41–45.
13. Wu H (2013) Higher-order assemblies in a new paradigm of signal transduction. *Cell* 153:287–292.
14. Wu B, et al. (2013) Structural basis for dsRNA recognition, filament formation, and antiviral signal activation by MDA5. *Cell* 152:276–289.
15. Yin Q, et al. (2015) Structural biology of innate immunity. *Annu Rev Immunol* 33:393–416.
16. Wu H, Fuxreiter M (2016) The structure and dynamics of higher-order assemblies: Amyloids, signalosomes, and granules. *Cell* 165:1055–1066.
17. Lin SC, Lo YC, Wu H (2010) Helical assembly in the MyD88-IRAK4-IRAK2 complex in TLR/IL-1R signalling. *Nature* 465:885–890.
18. Tidow H, et al. (2007) Quaternary structures of tumor suppressor p53 and a specific p53 DNA complex. *Proc Natl Acad Sci USA* 104:12324–12329.
19. Goldschmidt L, et al. (2010) Identifying the amylome, proteins capable of forming amyloid-like fibrils. *Proc Natl Acad Sci USA* 107:3487–3492.
20. Li J, et al. (2012) The RIP1/RIP3 necrosome forms a functional amyloid signaling complex required for programmed necrosis. *Cell* 150:339–350.
21. Sawaya MR, et al. (2007) Atomic structures of amyloid cross-beta spines reveal varied steric zippers. *Nature* 447:453–457.
22. Sborgi L, et al. (2016) GSDMD membrane pore formation constitutes the mechanism of pyroptotic cell death. *EMBO J* 35:1766–1778.
23. Das S, et al. (2016) GSDMB induces an asthma phenotype characterized by increased airway responsiveness and remodeling without lung inflammation. *Proc Natl Acad Sci USA* 113:13132–13137.
24. Kumar DK, et al. (2016) Amyloid-beta peptide protects against microbial infection in mouse and worm models of Alzheimer's disease. *Sci Transl Med* 8:340ra72.
25. Rodriguez JA, et al. (2015) Structure of the toxic core of alpha-synuclein from invisible crystals. *Nature* 525:486–490.
26. De Simone A, et al. (2012) Intrinsic disorder modulates protein self-assembly and aggregation. *Proc Natl Acad Sci USA* 109:6951–6956.
27. Eisenberg D, Jucker M (2012) The amyloid state of proteins in human diseases. *Cell* 148:1188–1203.
28. Seuring C, et al. (2012) The mechanism of toxicity in HET-S/HET-s prion incompatibility. *PLoS Biol* 10:e1001451.
29. Anguiano M, Nowak RJ, Lansbury PT, Jr (2002) Protofibrillar islet amyloid polypeptide permeabilizes synthetic vesicles by a pore-like mechanism that may be relevant to type II diabetes. *Biochemistry* 41:11338–11343.
30. Lee JH, et al. (2013) Crystal structure and versatile functional roles of the COP9 signalosome subunit 1. *Proc Natl Acad Sci USA* 110:11845–11850.
31. Kabsch W (2010) Xds. *Acta Crystallogr D Biol Crystallogr* 66:125–132.
32. Winn MD, et al. (2011) Overview of the CCP4 suite and current developments. *Acta Crystallogr D Biol Crystallogr* 67:235–242.